Determination of the relative and absolute Seebeck coefficient of a thin Platinum layer

William Wenig[1], Yoshua Hempel[1], Olivio Chiatti[1,2]

[1]Institut für Physik, Humboldt-Universität, 12489 Berlin, Germany
[2]Supervision of lab course

In this advanced lab course we studied the Seebeck effect and familiarized ourselves with the working principle of a thermocouple and four-terminal probing to operate resistance thermometers. We utilized a microlab which consisted of sputtered thin Platinum films on top of a glass substrate and a bonded Gold wire. We performed our measurements in a closed-cycle cryostat in order to obtain the temperature dependent relative Seebeck coefficient of Platinum and Gold and used reference data to ultimately extract the absolute Seebeck coefficient of Platinum at four different temperatures. We compared our findings and preliminary results with parameters of the bulk material and drew conclusion as to why discrepancies arose.

The application of the Seebeck effect through the use of thermocouples, named after Thomas Johann Seebeck, who discovered it in 1821 [1], makes it possible to measure temperatures under conditions, where many other thermometers fail. This is mainly due to their ability to function at high temperatures, potentially exceeding 1000° C [2] and lack of moving parts. As the name suggests, a thermocouple always consists of two dissimilar conductive materials. These are connected at two junctions which are held at different temperatures. Two different materials are required, as otherwise the electromotive force over the voltmeter will cancel itself out, the measurable thermovoltage being proportional to the difference of their Seebeck-coefficients [3]. Examples of current research concerning thermocouples and the thermoelectricity of materials include studying how thermoelectric properties change for small dimensions, compared to the bulk materials, such as for thin films and nanowires [4]. Other research [5] is concerned with finding materials that exhibit a high figure of merit $ZT = S^2\sigma\kappa^{-1}T$, a dimensionless quantity, which positively correlates with device efficiency, as in its conversion factor from absorbed heat to usable energy. An ideal, thermoelectric material should then have a high Seebeck coefficient S and electric conductivity σ and low thermal conductivity κ in order to maximize ZT. This is a rare combination for conductive materials, as for example the Wiedemann–Franz law states that in the free-electron model $\kappa\sigma^{-1} = LT$, with the Lorentz number L, resulting in $ZT = S^2L^{-1}$.

In this work we showcase how we evaluated data

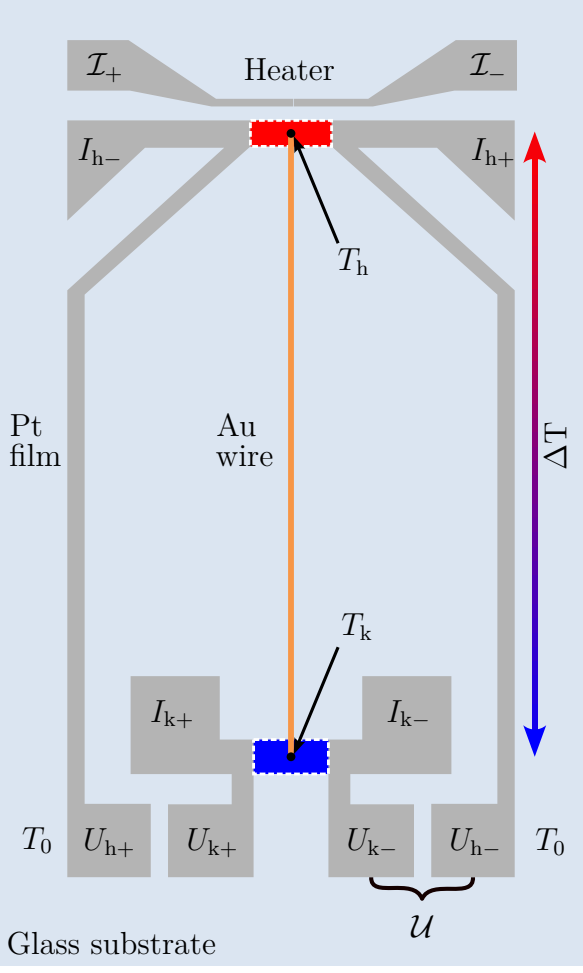

Figure 1 | The sample consists of three thin Platinum films deposited onto a substrate by thermal evaporation and a Gold wire bonded to two contact points. The platinum was deposited onto three separated regions of the substrate. The topmost region acts as a microheater, while the other ones are the hot and cold thermometer of the Platinum's half of the thermocouple, which are connected by the Gold wire. Recreated illustration from figure 1a [6].

obtained with a Platinum-Gold thermocouple to determine its relative Seebeck-coefficient at four temperatures. Regrettably the data we used wasn't obtained by us, as we ran into technical difficulties with the setup of the experiment. In the following, we make the assumption that the data was obtained in the same way as we were instructed to. The data was obtained using a Seebeck platform, as shown in figure 1, which was inserted into a vacuum chamber for thermal insulation. As a precaution to not falsify the measurements by damaging the sample, we grounded ourselves and used an ITC 16A IC Test Clip which short circuited all the Seebeck-platform's contacts. The measurements were done at a pressure in the region of 10^{-6} mbar, reached with the help of a turbomolecular pump.

For controlling the bath-temperature T inside the chamber we utilized the DE-202A-DMX-20 closed cycle cryostat from Advanced Research Systems Inc. With the help of this cryostat, a desired bath-temperature was set, at which current-voltage characteristics of the two thermometers in the Seebeck-platform were measured. These are resistance thermometers in the four-terminal configuration to achieve a high accuracy in both voltage and current. Next, a current $\mathcal{I}$ of 1 mA was applied to the platform's microheater and after waiting a while to ensure a steady state was reached, the current-voltage characteristics of the thermometers were measured again, as well as the thermovoltages. The process of incrementing the heating current $\mathcal{I}$ by 1 mA was repeated up until a current of 9 mA. After this a new bath-temperature was set and we repeated the process.

The collection of data was mostly handled by a program built in labview, which automated the measurement of current-voltage characteristics and thermovoltages. This was made possible by a Keithley 7001 Switch Matrix providing an interface, through which the circuit could be controlled from the computer.

1 Establishing an overview

Performing the analization and arriving at the final results required us to process our obtained data in multiple steps. Many of these steps require input in the form of results from preceding steps, which renders the analysis convoluted. The illustration in figure 2 follows the general structure of a block-flow diagram which we found to be very useful to construct the programmatic implementation of the analysis in Python. Each box represents a processing step that requires inputs and yields outputs. Input and output are represented by arrows pointing into the in- or outward direction of the respective box. Before an arrow arrives at a box it originates from a rhomboid or a circle with the quantity for

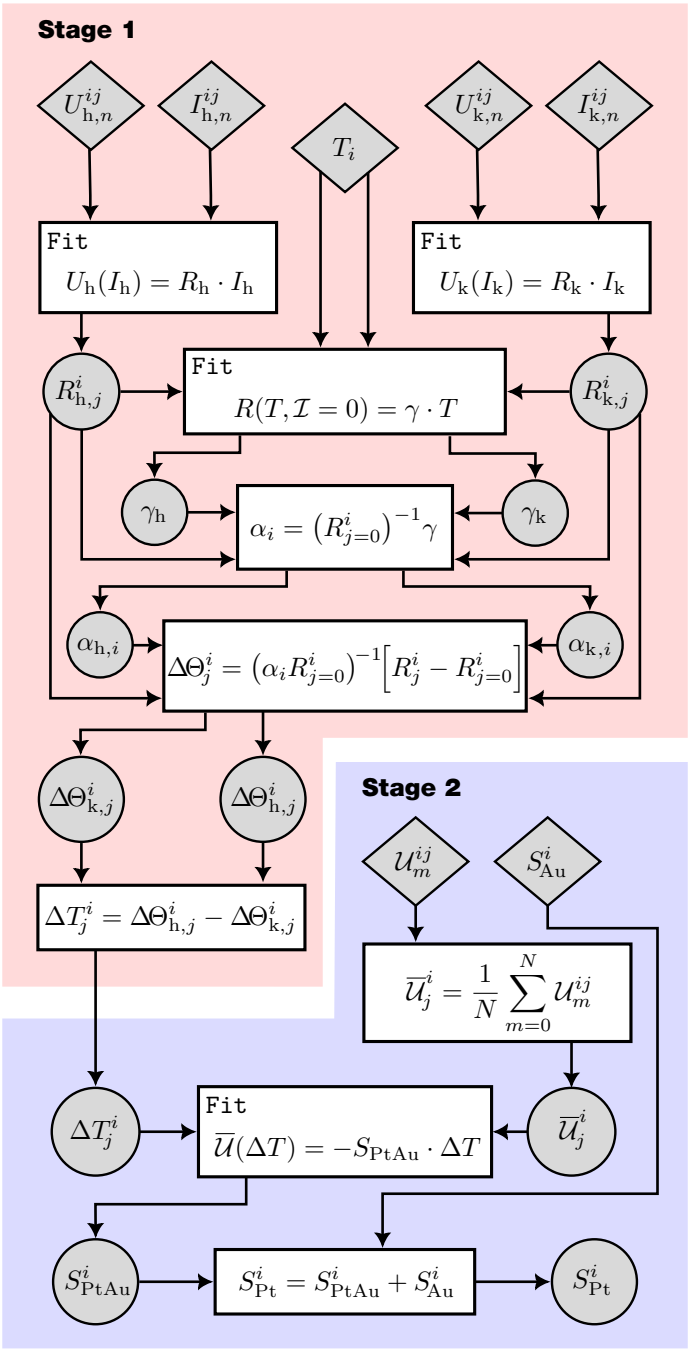

Figure 2 | The data is involved in an analysis with two stages consisting of multiple regressions and combinations. Overview illustrating how the raw data (rhombi) went through different stages of preliminary results (circles) by transformations (rectangles). We combined the preliminary results and performed linear regressions upon them to obtain our final result $S_\mathrm{Pt}(T)$. The overall analysis is broken into two stages denoted by the red and blue boxes.

which the arrow represents the input. Analogously arrows representing output from a method always arrive at circles which represent a preliminary or final result. The rhomboids and circles represent quantities inside of which each of them is quoted with a set of indices.

We use these sets of indices as addresses that indicate the bath temperature T_i and heating current $\mathcal{I}_j$ of the data point or data set. The indices n and m are used for data sets gathered during a sweep or for repeated measurements respectively. For example the voltages $U^{ij}_{\mathrm{h},n}$ were gathered, sweeping the currents $I^{ij}_{\mathrm{h},n}$ and the $\mathcal{U}^{ij}_m$ are repeated measurements at the same bath temperatures T_i and heating currents $\mathcal{I}_j$.

We broke down the analysis into two main stages. Stage 1 concerns the determination of the total temperature differences ΔT^i_j between the hot and cold Pt-Au-interface regions depicted in figure 1. In this stage, data from the hot and cold thermometer are processed by the same methods which is why we dropped the indicating indices inside all boxes that have *two* output arrows. In stage 2 the results for the ΔT^i_j are used for determining the relative Seebeck coefficients S^i_{Pt} which ultimately yields the absolute Seebeck coefficients S^i_{Pt} for all of our bath temperatures T_i.

It is important to note that the position of the indices of our quantities do not convey any mathematical structure. We write $U^{ij}_{\mathrm{h},n}$ rather than $U_{\mathrm{h},ijn}$ because it allows for a more compact notation. Furthermore all operations between quantities in figure 2 are to be understood as element-wise. Our block-flow diagram only represents the main processing steps to arrive at the final results S^i_{Pt} and does not contain the methods which construct the uncertainties of our quantities.

2 Uncertainties of the data

Before we examine the results of each stage, we have to discuss the systematic and random uncertainties in the data. From the overview in figure 2 it is visible that we obtained data for seven different quantities of which the absolute Seebeck coefficients of Gold S^i_{Au} were not measured.

We will start with the description of the uncertainties in the thermovoltages $\mathcal{U}^{ij}_m$. For measuring all voltages we utilized the Keithley 2182A Nanovoltmeter in a range of $\mathcal{U}_{\max} = 100$ mV. As specified [7] for thermovoltages given in Millivolts, the systematic error is

$$s^i_j = 10^{-6}\left[(40+30)\,\mathcal{U}^{ij}_m + (5+30{\cdot}0.2)\,\mathcal{U}_{\max}\right] \qquad (1)$$

where the second and fourth term originates from a temperature coefficient of the systematic error which corrects for the behavior of our voltmeter operating on a temperature of 30 °C. For the random uncertainty we introduce the standard errors ε^i_j [8]

$$\varepsilon^i_j = \frac{\sigma^i_j\left(\mathcal{U}^{ij}_m\right)}{\sqrt{N}} = \sqrt{\frac{1}{N(N-1)}\sum_{m=0}^{N}\left(\mathcal{U}^{ij}_m - \overline{\mathcal{U}}^i_j\right)^2} \qquad (2)$$

where the $\sigma^i_j\left(\mathcal{U}^{ij}_m\right)$ are the standard deviations of the repeated measurements. We combine systematic and random uncertainty by Pythagorean addition (see [9], figure 12) to

$$u^i_{\mathcal{U},j} = \sqrt{\left(s^i_j\right)^2 + \left(\varepsilon^i_j\right)^2}. \qquad (3)$$

Finally we want to check how the $\mathcal{U}^{ij}_m$ are distributed. For each bath temperature T_i and heating current $\mathcal{I}_j$ we gathered $N = 10$ repeated measurements of $\mathcal{U}$. This sample size is insufficient for revealing the shape of the parent distribution. If we neglect the dependence of the parent distribution on T and $\mathcal{I}$ and transform the measurements in order to compare them to each other, the sample size increases to the number of measurements of $\mathcal{U}^{ij}_m$ across *all* indices. We chose to transform the data into normalized deviations from their means using the $\overline{\mathcal{U}}^i_j$ and σ^i_j. The visual inspection of this approach through figure 3 confirms the hypothesis that the $\mathcal{U}^{ij}_m$ are normally distributed.

The uncertainties related to the voltages $U^{ij}_{\mathrm{h},n}$ and $U^{ij}_{\mathrm{k},n}$ are built in a similar manner. The systematic error results analogously from equation (1), as these voltages were measured with the same experimental setup. The random error and shape of their distribution are not accessible because we did not conduct repeated measurements for these quantities. We will estimate the random error by reusing the ε^i_j of the $\mathcal{U}^{ij}_m$

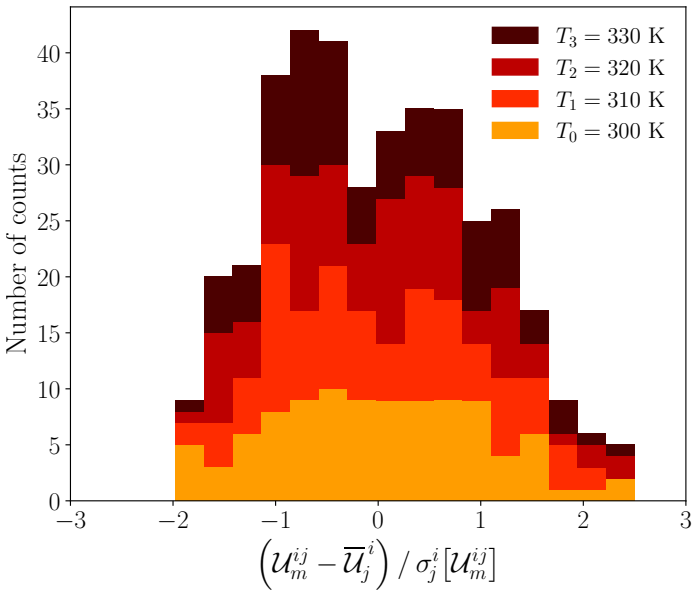

Figure 3 | The normalized deviations from the means reveal a general agreement with a normal distribution. Histogram of the normalized deviations from the means of the $\mathcal{U}^{ij}_m$ for all bath temperatures T_i and heating currents $\mathcal{I}_j$. Furthermore each contribution to the number of counts from all T_i are illustrated by color graduation.

from equation (2) and therefore assume the data follows a normal distribution.

As we have measurements for the heating currents $\mathcal{I}_j$ from the Keithley Sourcemeter 2401 and for I_h and I_k from the Keithley Source 6221, we know their systematic uncertainties. But we did not conduct any repeated measurements, which leaves us with no acceptable random uncertainty or shape of distribution. We chose to perform least-squares regressions with uncertainties in the *dependent* variable. This discards the uncertainties in all currents because they only contribute to the analysis as *independent* variables.

We utilized the Lake Shore Cryotronics Model 335 temperature controller for collecting and controlling the bath temperature T. Two sensors inside the cryostat provided the input for the controller. The T_i are values corresponding to measurements from the sensor closest to the probe. As we have no further information about the sensors inside the cryostat we also discarded the uncertainties in this quantity by the procedure applied to the currents. The reference values S_Au represent a special case and their uncertainties will be discussed in the following section.

All other uncertainties related to quantities from circles in figure 2 result from errors in fit parameters or propagation. Because of the overall convolution in the analysis we explicitly dismiss statistical correlation between quantities for error propagation in stage 1 as this would exceed the scope of this report.

3 Data processing and results

The main result of this work is the temperature dependent, absolute Seebeck coefficient of the thin platinum film $S_\mathrm{Pt}(T)$ for four bath temperatures T_i. But processing our data, with the workflow from figure 2, also returned other useful characteristics of the platinum film. In this section we will present these preliminary and final results and compare some of them with reference values of the bulk material.

The first step of stage 1 is determining the temperature dependent resistances R_h and R_k which correspond to the platinum films of the hot and cold thermometer depicted in figure 1. With temperatures reaching only from 300 K to above 330 K, Ohm's law holds hence we utilized it for working out the resistances for four bath temperature T_i at ten different heating currents $\mathcal{I}_j$. We exemplify this procedure on our set of measurements with no heating current $\mathcal{I}_0 = 0$. The temperature dependence of the resistances R_h and R_k are clearly visible from figure 4 as the slope of the current-voltage characteristic increases for an increasing bath temperature. Both thermometers exhibit this trend, but alter in their total resistances

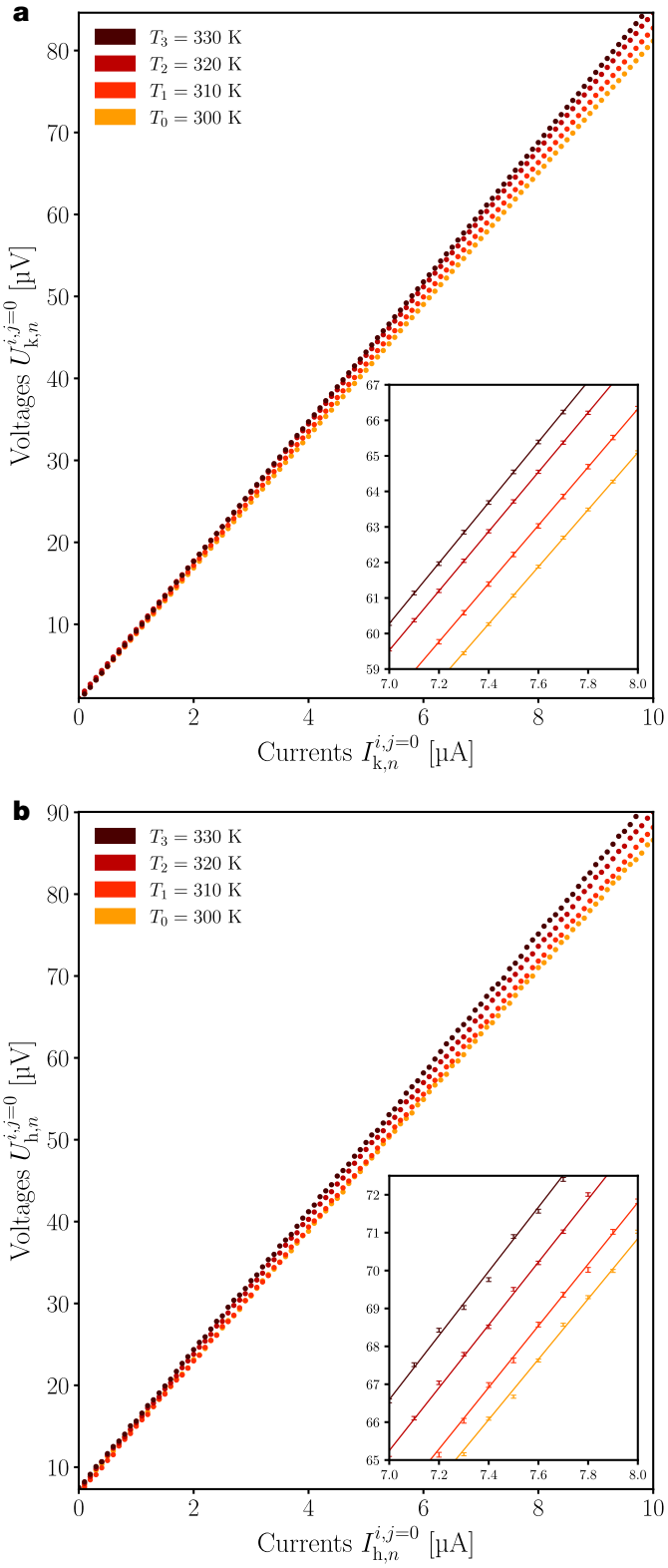

Figure 4 | Current-voltage characteristics reveal the temperature dependent resistance of the platinum films. Linear regressions of the data from current sweeps at all bath temperatures T_i with no heating currents. The measured voltages and currents originate from the platinum films which are used as the **a)** cold and **b)** hot thermometer on the substrate. Best fit lines and error bars are hidden for visual clarity but displayed in a smaller inset.

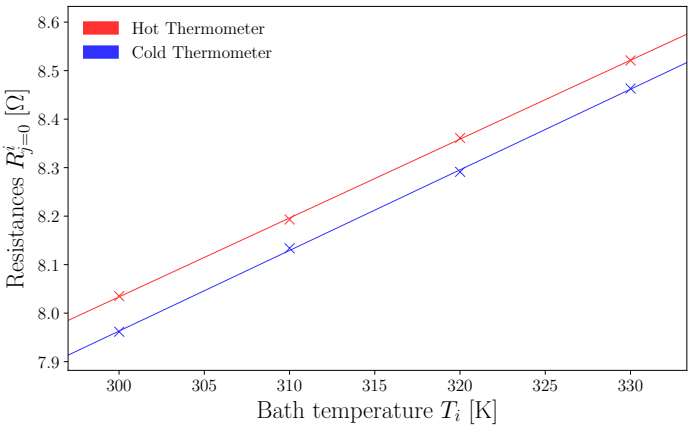

Figure 5 | The resistances R_h and R_k are separated by a gap for all T_i and exhibit a linear dependence on temperature. Resistances R of the hot and cold thermometer for all bath temperatures for no heating current with a best fit line. The resistances result from the linear fits of the thermometers the current-voltage characteristics.

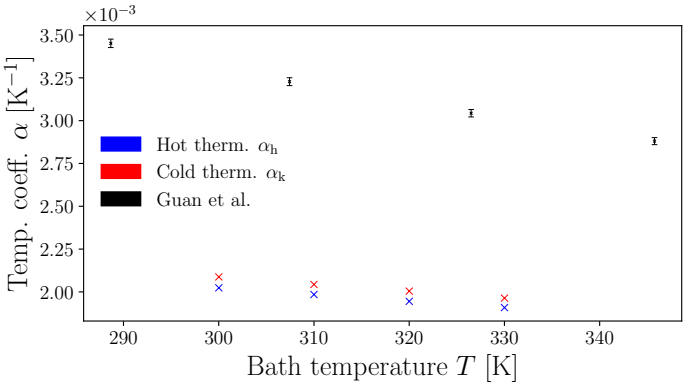

Figure 6 | The temperature coefficients we obtained do not stand in agreement with reference data from the bulk material Obtained temperature coefficients (red and blue) of our platinum films with reference values from the bulk material.

as all current-voltage characteristics of the hot thermometer in figure 4b) have a smaller slope than the cold thermometer in 4a). This can be traced back to the differing size of the probe or interaction area which are illustrated in figure 1 as red and blue squares. Although we depict these areas in roughly equal sizes in the illustration we think that the areas of the platinum film, for which the four-terminal method measures the resistances, vary for both thermometers because of their complicated and unequal geometry. We also visualized the calculated resistances $R_\mathrm{h}(T)$ and $R_\mathrm{k}(T)$ for $\mathcal{I}_0$ in figure 5. The gap between R_h and R_k for all bath temperatures can be observed more clearly from there.

From the resistances at no heating current we obtained the temperature coefficients of the resistance α_h for the hot thermometer and α_k for the cold thermometer. The first order expansion of the temperature dependent resistance $R(T)$ around a particular reference temperature T_i is

$$R(T) = R_i(T_i)\Big[1 + \alpha_i(T - T_i)\Big]. \tag{4}$$

The expansion coefficient α_i (temperature coefficient) is calculated from

$$\alpha_i = \frac{1}{R_i(T_i)} \frac{\mathrm{d}R(T)}{\mathrm{d}T}\Big|_{T=T_i} = \Big[R_i(T_i)\Big]^{-1} \cdot \gamma_i, \tag{5}$$

from which we can observe that the temperature coefficient is dependent on a reference temperature around which the behavior of $R(T)$ is approximated. For our calculation we approximated the γ_i from equation (5) with the slope of the best fit lines γ_h and γ_k in figure 5 and used the $R^i_{\mathrm{h},j=0}$ and $R^i_{\mathrm{k},j=0}$ as $R_i(T_i)$. Plugging these quantities into equation (5) results in a total of eight temperature coefficients $\alpha_{\mathrm{h},i}$ and $\alpha_{\mathrm{k},i}$. We displayed them in figure 6 with reference values of the bulk material from Guan et al. [10]. We obtained the reference values by fitting to data from their high temperature resistivity measurements. From figure 6 we can see, that our obtained values and the references exhibit the same trend for increasing bath temperatures. The reference values cannot be readily compared to our values as they do not exactly match each others reference temperatures. We can still notice that there is a significant gap between the reference values and our obtained results. We think that this is due to the fact that at temperatures above the Debye-temperature $\theta_\mathrm{D} = 240$ K electrical conductivity is mainly limited by electron-phonon scattering [6]. The number of phonon modes in the acoustical branch depends linearly on the number of unit cells in the crystal hence the increase in occupied phonon modes for higher temperatures is larger in the bulk material than in the thin film. The probability of electron-phonon scattering increases for a larger number of occupied (or multiply occupied) states of phonons.

Lastly we perform the last step of stage 1 from figure 2. We calculated the temperature differences on the probe areas of the hot and cold thermometer $\Delta\Theta^i_{\mathrm{h},j}$ and $\Delta\Theta^i_{\mathrm{k},j}$. They follow from the linear expansion of the temperature dependent resistance in equation (4) and are used to build the total temperature difference between the two thermometers ΔT^i_j for all bath temperatures T_i and $\mathcal{I}_j$.

Now we will conclude the analysis with the results of stage 2. We can plot the thermovoltages $\overline{\mathcal{U}}$ with

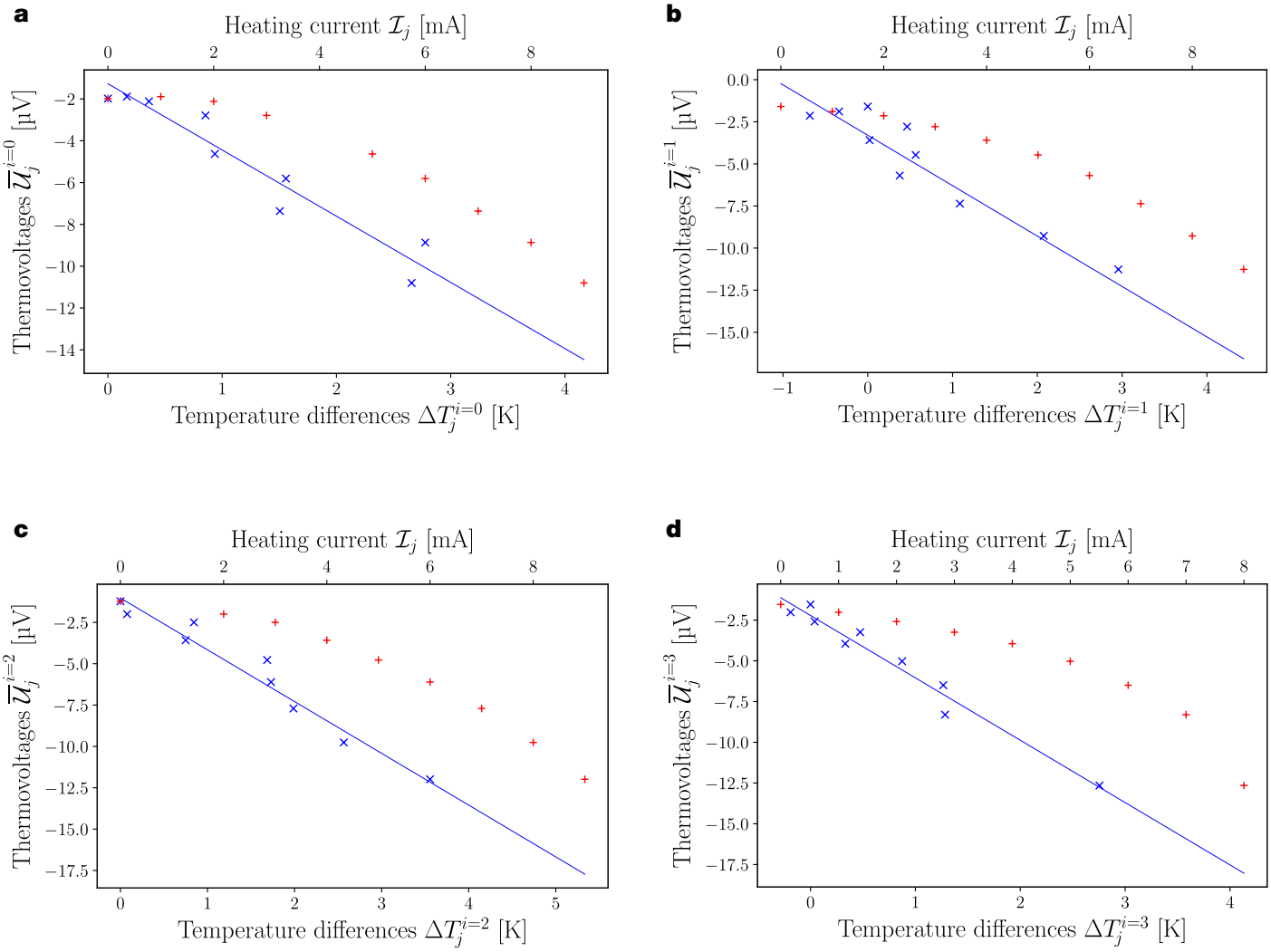

Figure 7 | The transition of the independent variable from the heating currents $\mathcal{I}_j$ to the achieved total temperature differences ΔT_j^i linearized the thermovoltages $\overline{\mathcal{U}}_j^i$. Thermovoltages $\overline{\mathcal{U}}_j^i$ in dependence of heating currents $\mathcal{I}_j$ (red) and temperature differences of the thermometers ΔT_j^i (blues) for all bath temperatures T_i and best fit line (blue). Error bar are hidden due to their small size.

the heating currents $\mathcal{I}_j$ and with the calculated temperature differences of the thermometers ΔT_j^i. This is visualized in figure 7. Generally we observe a quadratic dependence of the thermovoltages on the heating currents and a linear dependence on the ΔT_j^i. If we assume that the heat flux of the system is in a stationary state, then it will be linearly dependent on the heating power $\mathcal{P} = \mathcal{R} \cdot \mathcal{I}^2$ and therefore explain the observed dependence. The linearization follows from the defining relation of the Seebeck coefficient $\mathcal{U} = -S \cdot \Delta T$. From figure 7 we can also observe that the calculation of ΔT_j^i yields negative values. This means that at this particular heating current the cold thermometer experienced a bigger temperature increase that the hot thermometer. If the system is not the aforementioned stationary state of heat flux, the global temperature gradient of the probe will follow a non-isotropic form. The waiting times for each measurement have to be at sufficient levels to ensure this condition. We suspect that the waiting times in our measurements were not sufficiently configured.

With the defining relation of the Seebeck coefficient we can extract the relative Seebeck coefficient of Platinum and Gold S_{PtAu} from our measurements. The best fit lines in figure 7 visualize this procedure. The last step is to calculate the absolute Seebeck coefficient of Platinum S_{Pt} from the relative Seebeck coefficient. For this we utilized the absolute Seebeck coefficient of Gold from Kockert [11]. In our temperature regime, the Seebeck effect is governed by thermodiffusion hence we extrapolated the data linearly.

We present the final results in figure 8 with reference values for S_{Au} and for the absolute Seebeck coefficient of the bulk material $S_{\mathrm{Pt,Vol}}$ from Guan et al. [10]. We notice that the reference values we picked share properties. They either increase (S_{Au}) or decrease

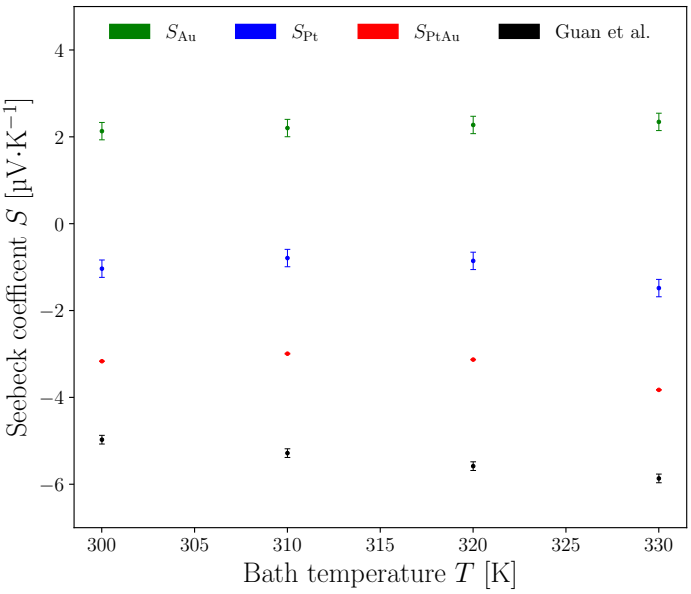

Figure 8 | The calculated Seebeck coefficients cannot reproduce the trend exhibited by the reference values but share its sign. Calculated and reference values for the absolute and relative Seebeck coefficients of Platinum and Gold.

monotonously ($S_{\mathrm{Pt,Vol}}$) which is not the case for the data we calculated. The calculated S^i_{PtAu} do not exhibit this monotonous behavior. We think that this can be traced back to the stability regarding the heat flux on the probe. If no stationary state is reached we obtain erroneous values for ΔT^i_j. This is especially significant for the bath temperature $T_{i=1} = 310$ K, where the negative deviations are the biggest. The best fit will minimize the distance to all data, which will yield an increased slope if for a larger number of data with $\Delta T^i_j < 0$.

We also notice that the $S_{\mathrm{Pt,Vol}}$ and S_{Pt} differ significantly from each other, similar to the temperature coefficients in figure 6. They differ in magnitude but are both smaller than zero. From the matching sign of the Seebeck coefficients we can conclude that our data reproduces the major carrier type of Platinum which are negatively charged. We think that the fact $\left|S_{\mathrm{Pt}}\right|$ is smaller than $\left|S_{\mathrm{Pt,Vol}}\right|$ is explained by the confinement along one dimension of the sample. Decreasing the thickness of the sample will increase the probability for surface and boundary scattering [6] and will ultimately reduce the magnitude of the Seebeck effect in the material as the charge carriers form the thermovoltage.

Conclusion

While preparing, conducting and analyzing the data of this advanced lab course we learned a lot about the experimental setups which can be used to study transport phenomena in solid state physics. We also learned about the difficulties when trying to extract temperature dependent physical quantities from measurements. With the thermocouple from figure 1 we were able to obtain the relative Seebeck coefficient of a thin Platinum film and a Gold wire and the absolute Seebeck coefficient of this Platinum film.

We could also convince ourselves of the difference in transport properties of a thin film and bulk material and gave estimates to the origin of this phenomenon.

References

1. Seebeck, T. J. Ueber die magnetische Polarisation der Metalle und Erze durch Temperaturdifferenz. *Annalen der Physik* **82,** 253–286 (1826).
2. Ripple, D. C. & Burns, G. W. Standard reference material 1749: Au/Pt thermocouple thermometer. *NIST Special Publication,* 260–134 (1998).
3. Fischer, S. F. & Kockert, M. *Bestimmung des relativen und absoluten Seebeck-Koeffizienten einer dünnen Platinschicht* Humboldt-Universität zu Berlin (AG Neue Materialien, 2018).
4. Kockert, M. E. Thermoelectric transport properties of thin metallic films, nanowires and novel Bi-based core/shell nanowires (2021).
5. Beekman, M., Morelli, D. T. & Nolas, G. S. Better thermoelectrics through glass-like crystals. *Nature materials* **14,** 1182–1185 (2015).
6. Kockert, M. E., Mitdank, R., Zykov, A., Kowarik, S. & Fischer, S. F. Absolute Seebeck coefficient of thin platinum films. *Journal of Applied Physics* **126** (2019).
7. *Model 2182 - Nanovoltmeter Instrument Specifications* Keithley Instruments (2016).
8. Hughes, I. & Hase, T. *Measurements and their Uncertainties: A Practical Guide to Modern Error Analysis* ISBN: 978-0-19-956632-7 (Oxford University Press Inc., 2010).
9. Müller, U. *Physikalisches Grundpraktikum: Einführung in die Messung, Auswertung und Darstellung experimenteller Ergebnisse in der Physik* (2007).
10. Guan, A., Wang, H., Jin, H., Chu, W., Guo, Y. & Lu, G. An experimental apparatus for simultaneously measuring Seebeck coefficient and electrical resistivity from 100 K to 600 K. *Review of Scientific Instruments* **84,** 043903 (Apr. 2013).
11. Kockert, M. E. *Thermoelectric transport properties of thin metallic films, nanowires and novel Bi-based core/shell nanowires* PhD thesis (Humboldt-Universität zu Berlin, Mathematisch-Naturwissenschaftliche Fakultät, 2021).